

# 3D inverse modeling of electrical resistivity and chargeability data through unstructured meshing, a case study for travertine exploration

Mohammad Ali Talebi <sup>a</sup>, Seyed Hossein Hosseini <sup>b</sup>, Maysam Abedi <sup>a,\*</sup>, Ali Moradzadeh <sup>a</sup>

<sup>a</sup> School of Mining Engineering, College of Engineering, University of Tehran, Iran.

<sup>b</sup> Institute of Geophysics, University of Tehran, Tehran, Iran.

## Article History:

Received: 16 August 2022.

Revised: 01 November 2022.

Accepted: 03 November 2022.

## ABSTRACT

Geoelectrical methods are considered common subsurface geophysical imaging tools that provide significant insight into the electrical properties of targets. Considering the three-dimensional nature of subsurface structures, geoelectrical survey data and their 3D inverted models can yield reliable and accurate results. In this research, using an unstructured tetrahedral meshing, three-dimensional forward and inverse models of electrical resistivity and chargeability data were performed for geological structures with travertine layers. The Application of the unstructured mesh for the discretization of subsurface geological units increases the speed and accuracy of the modelling procedure, as well as the flexibility in designing and implementing meshing on tough topographies and the complex-shaped geometry of the target mass. Using an open-source and full-item Python software named ResIPy, the forward and inverse models were calculated and interpreted precisely. According to the geological background of the studied area, to investigate the applicability and efficiency of the 3D geoelectrical modelling method in imaging the subsurface travertine deposits, three synthetic scenarios were modeled according to the geological setting of the studied area. The results of the 3D inversion of the synthetic models indicated the accuracy and validity of this procedure in the exploration of underground travertine deposits. As a real case study, the electrical resistivity and chargeability survey datasets in the Atashkohe travertine mine were inverted in 3D, aimed to inferring schematic geological sections along the three surveyed profiles. The survey was conducted with electrode spacing of 10 and 15 meters, using a combination of dipole-dipole and pole-dipole arrays. Considering the two-dimensional nature of these data and the relatively large distance between the two main profiles, the three-dimensional inversion results may increase the error rate. Therefore, the 2D batch inversion was preferably utilized in order to obtain a more realistic and sensible geological model. According to the geological studies and instrumental analysis of the rock samples, three types of geological structures were identified throughout the study area. Based on the subsurface electrical characteristics inferred along each profile, three geological layers were designed to illustrate the underground structures. The comparison of the inferred geological models and the drilling results along one of the survey profiles demonstrated acceptable compatibility and concordance, indicating the efficiency of the research utilized approach.

**Keywords:** *Electrical resistivity, Chargeability, 3D inverse modeling, Atashkohe travertine, Unstructured mesh.*

## 1. Introduction

Electrical Resistivity Tomography (ERT) is a well-known and powerful tool for measuring the electrical properties of layers or rocks, especially in distinguishing between enriched and depleted rocks by measuring the electrical resistivity and chargeability [1,2]. The purpose of geoelectrical surveys is to determine the electrical properties of subsurface units through surface or borehole measurements. These measurements lead to the recoding of apparent resistivity and chargeability values of subsurface layers. The mentioned electrical properties depend on various characteristics of rocks, such as rock type, fluid content, porosity, and water saturation. Geoelectrical instruments have been utilized for several decades in different geoscientific fields, such as hydrogeology studies, mine explorations, geotechnics, and environmental studies [3-5]. In many cases, for the exploration of mineral deposits, the integration of multiple geophysical methods can have a significant impact on controlling ambiguities and the inherent non-uniqueness arising from the inverse modelling [6, 7]. Along with the proper determination of exploratory drilling locations in identifying blind targets, some factors, such as cost and time in the implementation of exploratory programs have also led to the widespread use of

geoelectrical surveys in shallow and deep exploratory studies [8, 9]. Due to the complexity of subsurface structures and arrangements, focusing on a single set of geophysical data can cause errors in geological interpretations. For this purpose, in many recent studies, a combination of electrical methods has been used to reduce interpretational errors, such as studying poly-metallic deposits, porphyry copper mineralization, manganese explorations, deposits of Au-Ag, identification of minerals alteration, and fault systems in rocks [ 6,7, 10-15].

Geoelectrics is a well-known practical geophysics technique for high-resolution shallow imaging of the subsurface layers which has recently been used in studies to investigate the building stones, such as marble, granite, and travertine. These studies include the use of electrical methods to identify and map fractures in marble mines to quickly distinguish the unfractured and broken areas [16, 17], using the ground penetrating radar method in spotting fractures, filled joints, and large blocks in granite mines [18], utilizing geoelectrics in recognition of geometry of the subsurface travertine structures [19, 20] and also applying geoelectrics in determining sinkholes and hidden karst caves

\* Corresponding author. E-mail address: [maysamabedi@ut.ac.ir](mailto:maysamabedi@ut.ac.ir) (M. Abedi).

within the travertine mines [21].

Since all geological structures are three-dimensional in nature, examining the three-dimensional electrical characteristics through a 3D interpretational model can provide the most accurate results in practice. Currently, three-dimensional surveys are being used in some studies; however, they have not reached a level of practicality to be commonly used like 2D approaches. The main reason for this, is the higher cost of 3D surveys compared to 2D ones in exploratory areas. The application of multi-channel sensors provides the possibility of capturing more than one point at a time and can also reduce the survey duration. 3D surveys along with the development of rapid computational tools make it possible to implement the inversion process over larger datasets, decreasing the duration of time spent in modeling procedure. These two factors make 3D inversions more practical. 3D surveys are mostly implemented through pole-pole, pole-dipole, and dipole-dipole arrays, because other arrays provide weaker coverage near the edges of the survey networks [23]. In addition, 3D geoelectrical methods consist of a wide range of applications, such as identifying bedrock boundary zones [24], investigating subsurface fluid flow [25] and monitoring landslide moisture dynamics [26].

Interpretation of the surveyed geoelectrical data requires the inversion procedure of these data to convert the raw measurements into an explicable distribution of electrical properties. In the company of an intuitive and user-friendly approach for geoelectrical data inversion using a graphical user interface (GUI), the "ResIPy" software has been developed as an open-source Python programming interface (API) (source code available in the GitLab repository at: <https://gitlab.com/hkex/pyr2>) [27]. The ResIPy graphical user interface facilitates the process of data entry, data filtering, and modeling of errors, meshing, data inversion, and plot of inverted models. This software applies the R2 and cR2 codes for 2D modelling and also uses the R3t and cR3t codes for 3D modelling of geoelectrical datasets [28]. For 3D modeling in the ResIPy software, the unstructured tetrahedral mesh is only applicable which is generated and supported by the Gmsh user interface [29] and the R3t and cR3t codes, respectively. A tetrahedral mesh consists of nodes and elements. Each element is defined by four nodes, and in addition, each electrode must occupy a single node. The elements near the electrodes have tiny sizes, and their sizes increase as they move away from the electrodes. This improves the modelling procedure in areas of the mesh where the density of the potential field is higher. On the other hand, increasing the size of the elements reduces the calculations and the amount of memory used by the computer. Compared to the structured meshing, the use of unstructured mesh has advantages in accurate geophysical modelling and the presence of very tough topographies. These advantages include the reduction of model parameters, the ability to build any topography, and also the capability to recover the targets with any geometry [30-32]. Within a three-dimensional space, Figure 1 depicts the differences between the structured and unstructured meshes, highlighting the advantage of the unstructured mesh in the discretization of complex-shaped targets.

## 2. Methodology

According to the geological characteristics of the travertine lenses in the study area, in this research, firstly, three 3D synthetics scenarios were forward-modeled and inverted. This simulation allows us to carefully check the ability of the electrical data modelling method to identify the desired travertine lenses. Then, the obtained data from the field survey in the Atashkohe travertine deposit were inverted in 3D.

### 2.1. 3D geoelectrical simulation of travertine lenses

To investigate and evaluate the applicability of the geoelectrical method in 3D modelling of travertine rocks, three synthetic scenarios with different structural characteristics were modeled. For the construction of all three models, five survey profiles with a distance of 20 meters on a sloping surface were assumed. The electrode distance in each profile was considered to be equal to 10 meters, and the dipole-

dipole array was used for the forward modeling. During the forward modeling process, 2% Gaussian noise was added to the electrical resistivity data as ambient noise in a real field survey.

In the first synthetic scenario, the target mass was placed at a depth of 10 meters as a travertine lens with dimensions of 20\*40\*60 meters, and also with the background resistivity and electrical chargeability values of 250  $\Omega\text{m}$  and 8 ms, respectively. The electrical resistivity and chargeability values of this mass were also considered to be equal to 2500  $\Omega\text{m}$  and 5 ms, respectively. The second synthetic model was created by adding a 10 m thick surface layer to the components of the first synthetic model. The electrical resistivity and chargeability values of this layer were equal to 1000  $\Omega\text{m}$  and 1 ms, respectively. Finally, the third synthetic model was made by adding another surface layer to the second one, and the electrical resistivity and chargeability values of this layer were equal to 500  $\Omega\text{m}$  and 2 ms, respectively. It should be noted that the main purpose of producing such a synthetic scenario is to investigate, in a reasonable manner, the ability of the 3D geoelectrical method to identify the layering and the underground target masses within the studied region through an unstructured meshing approach. The geoelectrical properties of the mentioned models are summarized in Table 1.

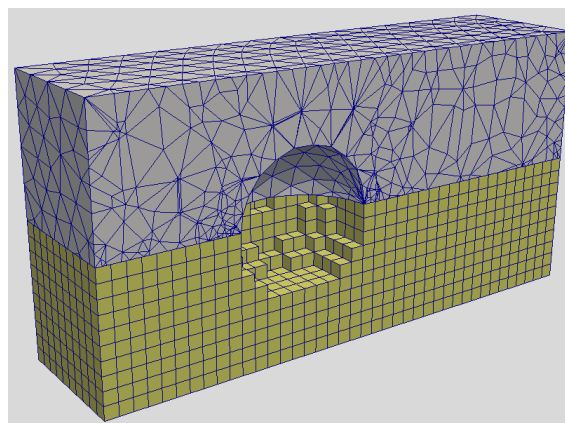


**Figure 1.** Physical model domain discretization with the structural and unstructured mesh [22].

**Table 1.** The geoelectrical properties of synthetic scenarios for simulation of the travertine occurrences.

Models	Model components	Resistivity ( $\Omega\text{m}$ )	Chargeability (ms)
Model 1	background value	250	8
	Target block	2500	5
Model 2	background value	250	8
	Target block	2500	5
	Layer 1	1000	1
Model 3	background value	250	8
	Target block	2500	5
	Layer 1	1000	1
	Layer 2	500	2

Each of the designed configurations in the presented synthetic models represents a structure of the travertine lens. Therefore, the background layer with low resistivity and high chargeability values was considered as the shale bedrock, the surface layer with high resistivity and low chargeability values was considered as the alluvial layer (conglomerate, sandstone, and travertine carcass stone), and the second layer with moderate resistivity and chargeability values was considered as the marl and conglomerate interlayer.

### 2.2. Geoelectrical inversion with unstructured mesh

The resultant data from the forward modelling of each of the synthetic models was inverted. Figures 2, 4, and 6 depict the real models

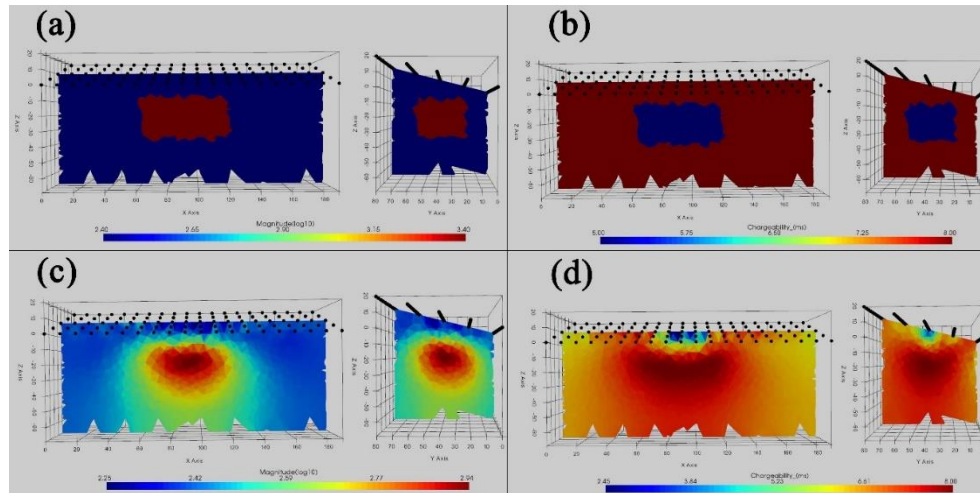


**Figure 2.** Synthetic model for the first scenario, (a) real model of the electrical resistivity, (b) real model of the electrical chargeability, (c) inverted model of the electrical resistivity, and (d) inverted model of the electrical chargeability.

of resistivity and chargeability with their inverted models along two vertical sections of the blocks of the synthetic models. Figures 3, 5, and 7 also present the apparent and predicted data of the electrical resistivity and chargeability after the forward and inverse modeling procedures of the synthetic models. Comparing the apparent and predicted data of electrical resistivity, no noticeable change or difference can be seen throughout the sections, indicating the high accuracy of the inverse modelling of the resistivity data. Regarding the chargeability sections, this comparison shows a slight difference in the range of data changes (smooth variations).

Examining the cross-sections resulting from the inversion data of synthetic model 1 (Figures 2c and 2d), the precision of the results is clearly evident and the recovered target block is well defined in the electrical resistivity cross-sections. Over the section of electric chargeability, a clear anomaly is observed in the center of the model, indicating the acceptable recovery of the target block, but with a mistaken value of a physical property. The chargeability model has also been affected by a low physical property contrast in comparison to the background setting assumed as shale material.

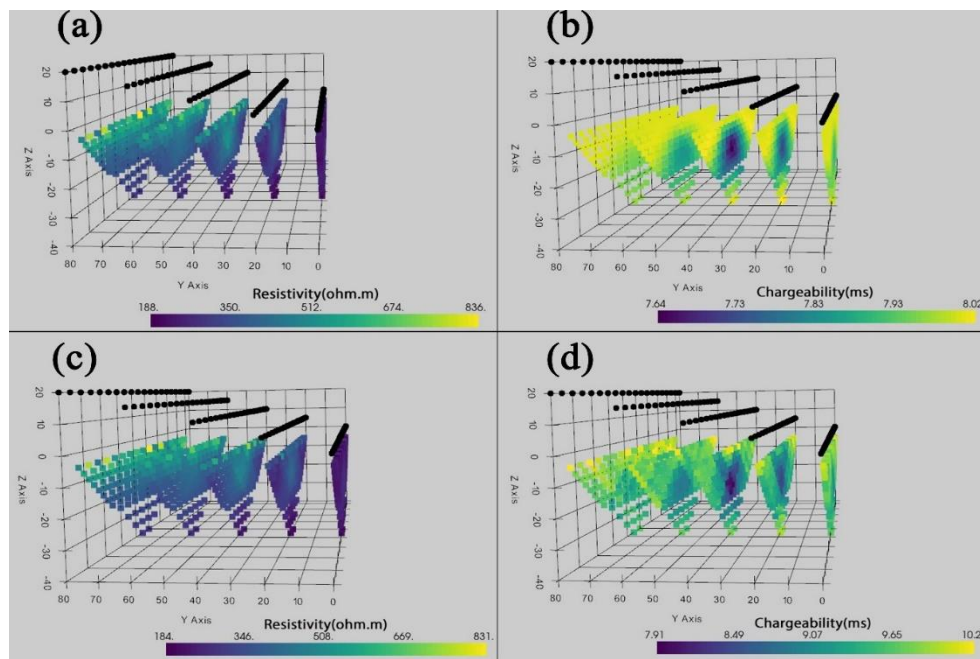


**Figure 3.** Geoelectrical data of synthetic model for the first scenario along the profiles overlaid by the topographic surface, (a) the observed apparent resistivity data, (b) the observed apparent electrical chargeability data, (c) the predicted electrical resistivity data, and (d) the predicted electrical chargeability data.

Considering the synthetic model 2, within the inverted model of electrical resistivity (Figure 4c), the target block and the surface layer are acceptably recovered and visible with good accuracy. In the inverted electrical chargeability model (Figure 4d), the surface layer is recovered accurately, but the target block, despite showing a good anomaly, is less detailed in terms of recovering the depth and dimensions of the block,

which is possibly affected by the conductive thin surface layer. However, the reliability and precision of the inverted models of the synthetic model 2 are evaluated at an acceptable level.

Within the inverted electrical resistivity model of the synthetic model 3 (Figure 6c), the two surface layers are well recovered and even the border between the two layers can be properly identified; while no

anomaly can be observed in the depth that can attributed as the target block, and the located block under the two mentioned layers is not properly recovered. In The inverted electrical chargeability model of the synthetic model 3 (Figure 6d), the surface layering is restored, while the boundary between the two layers is hard to distinguish. In identifying the target block, this model also performed poorly, and no exact anomaly was explicitly observed. Finally, the modeling of geoelectrical data in the synthetic model 3 worked well in identification of the surface

layering, while it was unable to identify the target block. Due to the thick surface conductive layer, the current density was very weak in the depth, and therefore, no valid trace was recorded within the geoelectrical data. From the geoelectrical data modelling, it can be concluded that in cases where the surface layers are not relatively thick or do not have significant conductivity, despite the extreme topography, the geoelectrical data modelling for travertine lens structures will be significantly fruitful and reliable.

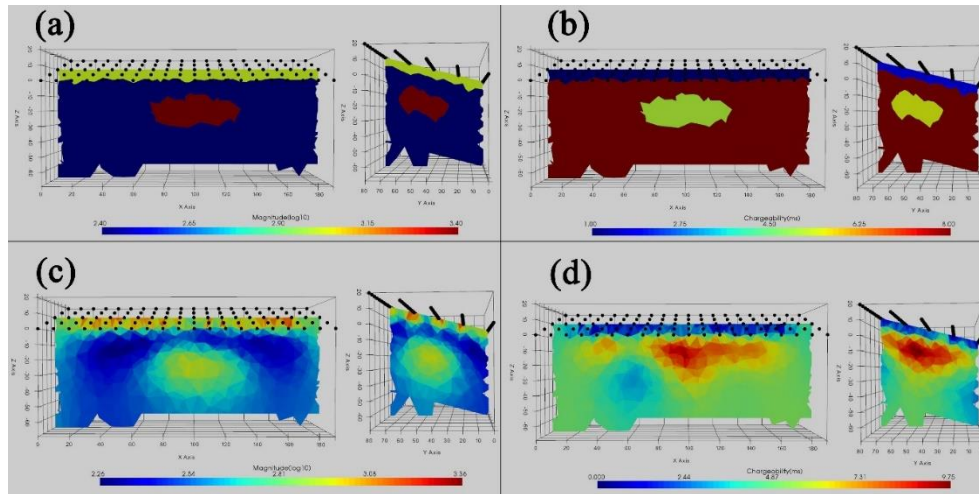


**Figure 4.** Synthetic model for the second scenario, (a) real model of the electrical resistivity, (b) real model of the electrical chargeability, (c) inverted model of the electrical resistivity, and (d) inverted model of the electrical chargeability.

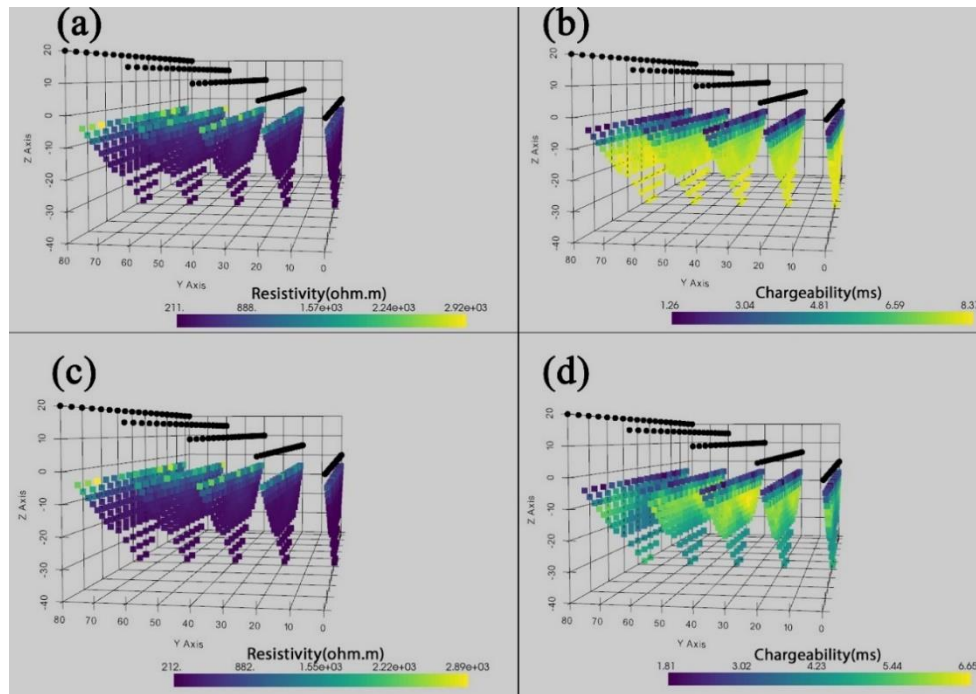


**Figure 5.** Geoelectrical data of synthetic model for the second scenario along the profiles overlaid by the topographic surface, (a) the observed apparent resistivity data, (b) the observed apparent electrical chargeability data, (c) the predicted electrical resistivity data, and (d) the predicted electrical chargeability data.

### 3. Geological setting of the study area

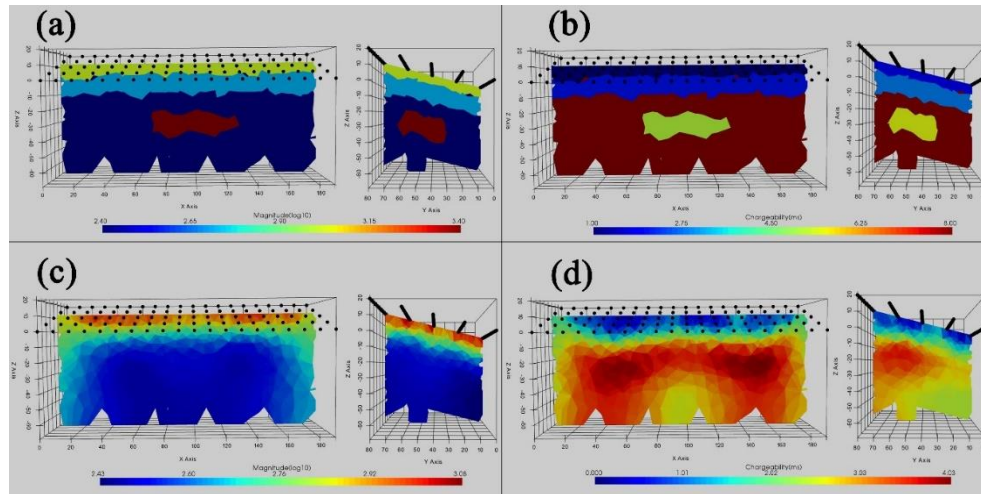
Iran consists of high mountain ranges and isolated mountainous areas, most of which have evolved during the third geological period, leading to huge resources of building stones. Geological maps of different regions in Iran show that this country has relatively high economic value in terms of mineral resources, especially building stones.

Figure 8(a) shows the distribution map of Iran's building stone mines, where the location of the studied area is specified concerning the general trend of the placement of the travertine mines.

The travertine zone of the Atashkohe is located in the northwest part of the 1:100,000 geological map of Dilijan and the 1:250,000 geological

map of Golpaygan. Among the exploratory area, shale, marl, sandstone, and conglomerate sequences along with limestone units are exposed in the west-east and northwest-southeast directions and their slope is also towards the northeast. As can be seen in Figure 8b, throughout the study area, the Plio-Quaternary travertine unit is widely placed with a low slope on the Jurassic shale and sandstone units in the southern and middle parts of the area, on the Cretaceous limestone and marl units in the northern middle part, and also on the Paleocene conglomerate unit in the northern part (Figure 8b). The thickness of the travertine layers, which are associated with the conglomerate, is different at every point of the study area. The thickness is relatively lower at the edges of the

travertine unit while increasing towards the middle. The layer thickness varies from 0.5 meters on the western edge up to 25 meters in the middle of the northern sectors. It's worth noting that the mentioned thickness of the travertine unit depends on the morphology of the bedrock in such a way that the conglomerate-travertine units have filled the pits of the primary surface morphology, and the thickness is higher in the locations of the previous valleys. By all means, the initial topography of the travertine layers has been tilted, and the slope of the deeper layers has been equal and in line with the direction of the topographic slope, while the shallower layers have relatively lower slopes [33].



**Figure 6.** Synthetic model for the third scenario, (a) real model of the electrical resistivity, (b) real model of the electrical chargeability, (c) inverted model of the electrical resistivity, and (d) inverted model of the electrical chargeability.

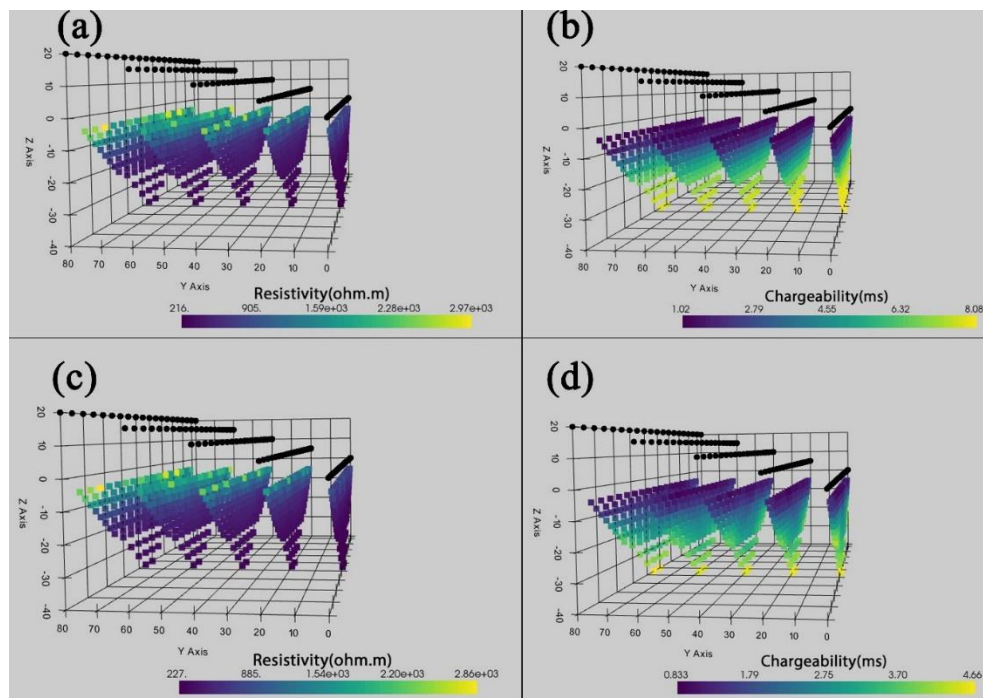


**Figure 7.** Geoelectrical data of synthetic model for the third scenario along the profiles overlaid by the topographic surface, (a) the observed apparent resistivity data, (b) the observed apparent electrical chargeability data, (c) the predicted electrical resistivity data, and (d) the predicted electrical chargeability data.

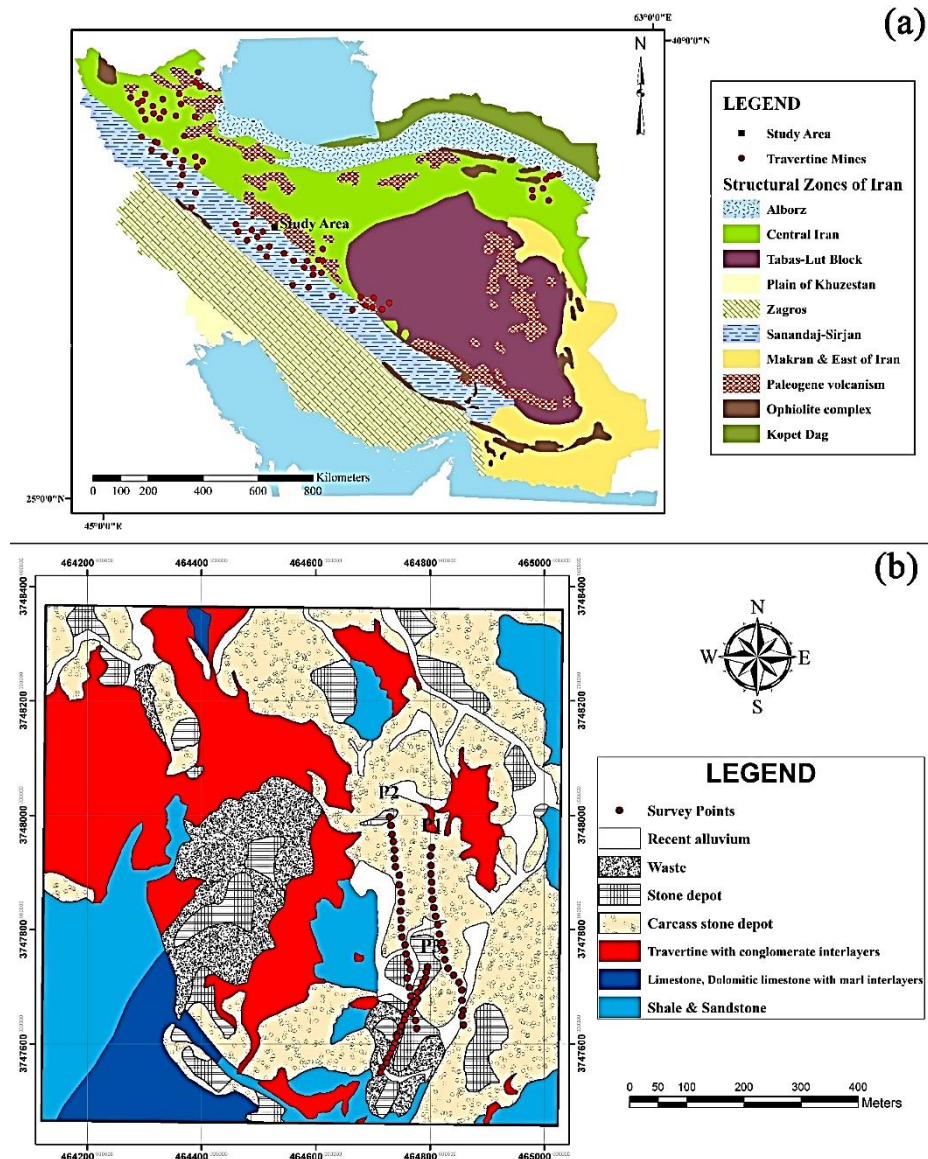
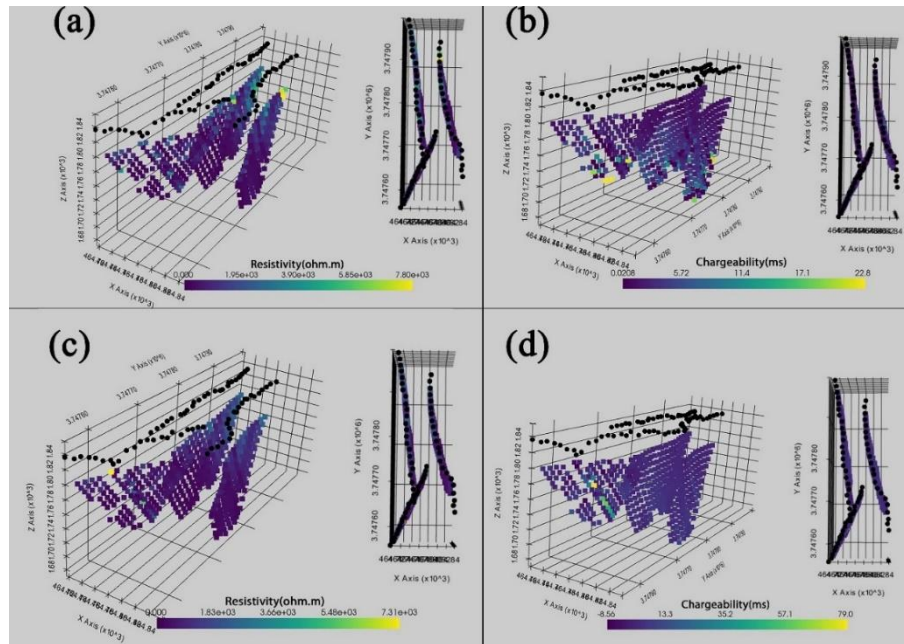


Figure 8. The distribution map of the building stones in Iran (a), and the detailed geological map of the Atashkohe travertine area (b) [31].

#### 4. 3D inverse modeling of geoelectrical data in the study area

To investigate the 3D inverse modelling of geoelectrical data using the unstructured meshing approach, the field survey data obtained from the travertine layers and outcrops in the Atashkohe were utilized. Considering the surface topography in this area and based on the nature of the travertine lens occurrences, three profiles were designed, and the electrical resistivity and chargeability surveys were carried out in two stages. The applied electrode arrangement in this study included a combination of dipole-dipole and pole-dipole arrays with an electrode spacing of 15 meters in the first phase of the survey operation, and a total of 550 readings were conducted within the study area along two profiles. In the second phase of the field survey operation, the third profile had a 10-meter electrode spacing, and a total of 300 readings were conducted. Figure 8b depicts a part of the geological map of the study area superimposed with the locations of the survey profiles. Since a 2D survey was conducted within the study area, three-dimensional survey data was not practically available. However, using the ResIPy software, 3D inversion of these data is possible.

In this research, the 3D inversion of the field data was performed using the unstructured meshing technique. As can be seen, the apparent and predicted data of the Atashkohe travertine area are shown in Figure 9. To be renotified, to properly discretize the modelling space, the unstructured tetrahedral meshing approach was used in this research to perform the 3D inversion process, which is depicted in Figure 10. The inversion scheme was run with seven iterations, and the RMS value was obtained equal to 6.86. The calculated inverted models are presented in Fig. 11. Figure 11a indicates the inverted model of the electrical resistivity along the transverse cross sections of the original model. Figure 11b also shows the electrical chargeability inverted model along the same sections of the original 3D model. As expected, the obtained models are associated with some error due to low survey data density and relatively tough topography, nevertheless, the geological layering status in the survey area can still be properly deduced. According to the inverted resistivity model, the geological layering of the area can be recognized well, and the surface layer with higher resistivity values can be identified. Therefore, the thickness of this layer is larger in the northern part of the model, and moving towards the south of the model, the thickness decreases. It shall be noted that the shale bedrock with low resistivity can also be recognized properly in the inverted model.



**Figure 9.** Geoelectrical data surveyed in the Atashkohe area, (a) the observed apparent resistivity data, (b) the observed apparent electrical chargeability data, (c) the predicted electrical resistivity data, and (d) the predicted electrical chargeability data. Data were displayed along three profiles.

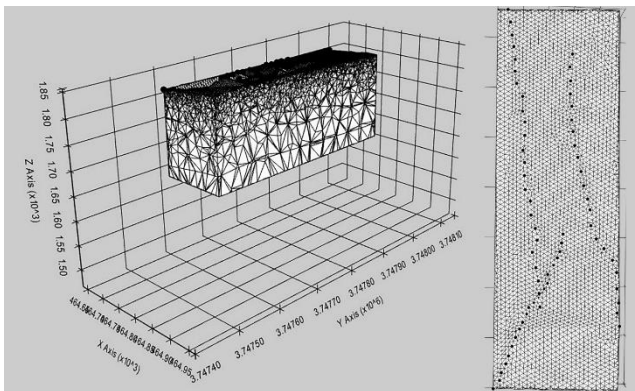


**Figure 10.** The unstructured mesh considered for subsurface discretization of the real physical model domain.

## 5. Geological interpretation

Using the geoelectrical inversion models, to provide a proper geological interpretation and investigate the underground features, some geological sections should be presented in line with the survey profiles. For this purpose, the two-dimensional batch inversion was utilized on the field data for the three profiles. As depicted in Figure 12, the inversion process produced models of electrical resistivity and chargeability along the three profiles. In addition, samples of travertine, bedrock, soil, and waste rock were collected from the Atashkohe mine, and their physical properties (electrical resistivity) were then determined by laboratory experiments. As can be seen, the results are presented in Table 2. Finally, four different types of structures were identified, including shale bedrock with low resistivity and high chargeability, a travertine layer with high resistivity, a layer containing conglomerate and dense sandstone with medium resistivity and chargeability, and a surface layer of soil and non-dense rubble with very high resistivity and low chargeability. According to the mentioned findings, a plausible geological model was prepared for each profile (Figure 13). As can be seen in the corresponding geological section (Figure 13c), the electrical measurements have been conducted over lenticular travertine outcrops along profile 3.

In the geological section of all three profiles, the existing layering within the area has been well demonstrated. Also, in the section of profile 1, at a distance of 120 meters from the origin and a depth of 15 meters, a travertine layer was specified, which was inferred from the presence of related anomalies in the area. To verify the results of the inversion process and provide a general view of the geology throughout the area, two drillings were conducted at distances of 105 and 165 meters from the first point of profile 2. The locations of these drilling points and the boundaries of the first layer in each drilling, marked in red, are shown in Fig. 13b. The depth of the first layer obtained from excavation and inverse modelling differs by a maximum of 1 meter, which indicates the acceptable application of the utilized electrical methods in identifying the layering in the study area. In cases with intact surface layers, it was also found that the applied electrical methods have acceptable accuracy in recognizing the geological situation and discovering plausible travertine layer.

## 6. Conclusion

This study evaluates the ability of the 3D inversion method using unstructured tetrahedral mesh to identify lenticular travertine structures for 3D synthetic models in the Atashkohe travertine area. The 3D forward and inverse modelling procedures were performed using the ResIPy program, which is an open-source tool scripted in Python programming language. This program facilitates data entry, data filtering, error modeling, meshing, data inversion, and inverse model presentation using a graphical user interface (GUI). The meshing cells were designed in a three-dimensional space in the form of unstructured tetrahedrons. This type of meshing formation leads to better modelling and understanding of the uneven topographic surfaces, reduces the model parameters, and facilitates the recovery of the target features with complicated geometries.

In this research, three 3D synthetic models were designed and modeled according to the possible geological structures of travertine layers. To generate the synthetic models, five sampling profiles with a distance of 20 meters were used, with each profile consisting of 20 electrodes with an electrode distance of 10 meters. The profiles were considered over a sloping surface. The electrode array used for 3D modelling was dipole-dipole, and a 2% Gaussian error was also added to the electrical resistivity data. The synthetic models contained layering

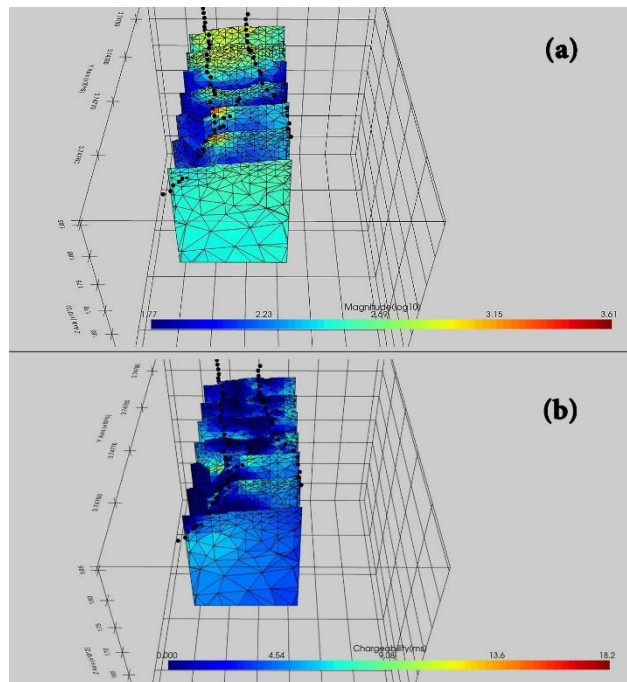


**Figure 11.** The inverse modeling 3D visualization of geoelectrical properties in the Atashkohe travertine area, (a) the electrical resistivity, (b) the electrical chargeability.

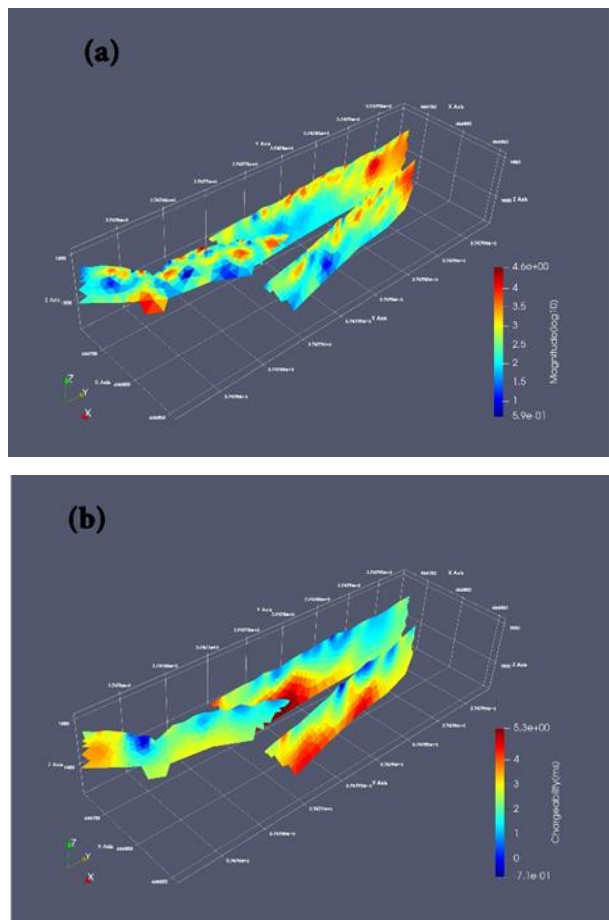


**Figure 12.** The visualization of electrical models along surveyed profiles, a) the electrical resistivity, b) the electrical chargeability.

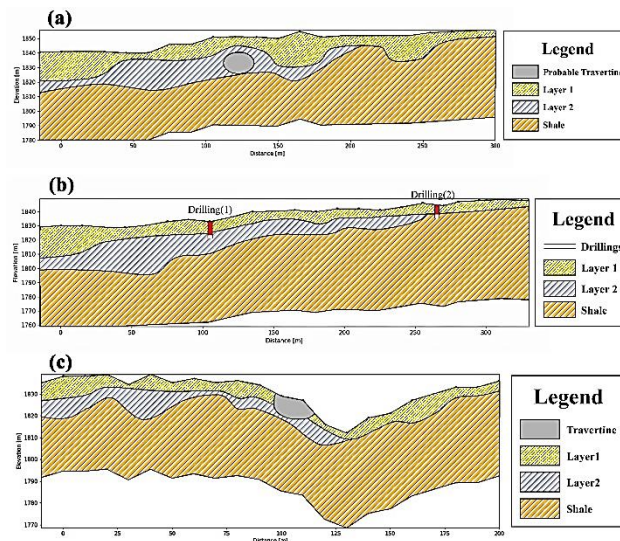


**Figure 13.** The schematic view of the proposed geological sections along three profiles 1 (a), profile 2 (b), and profile 3 (c).

**Table 2.** The Geoelectrical characteristics of sedimentary materials within the Atashkohe area based on the laboratory analysis along with general form of each material electrical property [34].

Layer	Measured resistivity ( $\Omega m$ )	Electrical resistivity within the study area ( $\Omega m$ )
Travertine	74	$50-10^7$
Mudy mid-layer	16-26	3-70
Shale Bedrock	619	20-2000
Soil and scree	95	-
Waste rock	76	1-100

and target mass in depth. The results of the 3D inverted modelling of the synthetic scenarios were acceptable and they were successful in the identification of the designed structures. According to the electrical modelling of the synthetic cases, despite the uneven topography and especially in cases with thinner surface layers and lower conductivity values, it was concluded that the identification of the lenticular travertine is properly possible through the modelling of geoelectrical data using the unstructured meshing approach.

As a case study, the geoelectrical data collected in the Travertine area of the Atashkohe were subjected to 3D inversion using an unstructured mesh. The data were collected in three profiles with a combination of pol-dipole and dipole-dipole arrays. The layering in the area was detected by examining the 3D inverted models. The surface layer with high resistivity was separated and identified from the bedrock with lower resistivity. The layer thickness values were higher towards the north of the model, decreasing towards the southern parts. Accordingly, three geological sections were deduced from the electrical models of each profile. In order to evaluate the efficacy of the applied geoelectrical method in this study, two boreholes were drilled along profile 2. The results indicate that the applied method was relatively accurate in identifying the structural boundaries of the study area. However, deeper excavations and drillings are required to accurately determine the plausible lenticular travertine layers.

### Acknowledgments

The authors are sincerely grateful to the Faravar Emdad Mining Company for its financial support, as well as to the referees and editors of the IJMGE Journal for their help in improving the quality of this article.

## REFERENCES

- [1] Gadallah, M.R., Fisher, R., & Mamdouh, R. (2009). *Exploration Geophysics*. Berlin: Springer-Verlag Berlin Heidelberg. doi: <http://doi.org/10.1007/978-3-540-85160-8>
- [2] Soleimani, K., Arab-Amiri, A. R., Kamkar Rouhani, A., Shamsaddini Nejad, M., & Momeni, F. (2019). Investigation of the accuracy of the results of geoelectrical surveys to determine the depth and thickness of bauxite layer in one of Jajarm bauxite deposits. *JOURNAL OF RESEARCH ON APPLIED GEOPHYSICS*, 4, 225-235
- [3] Aristodemou, E., & Thomas-Betts, A. (2000). DC resistivity and induced polarization investigations at a waste disposal site and its environments. *Journal of Applied Geophysics*, 44, 275-302
- [4] Binley, A., & Daily, W. (2003). The performance of electrical methods for assessing the integrity of geomembrane liners in landfill caps and waste storage ponds. *European Journal of Environmental & Engineering Geophysics*, 8, 227-237
- [5] De Carlo, L., Perri, M. P., Caputo, M. C., Deiana, R., Vurro, M., & Cassiani, G. (2013). Characterization of a dismissed landfill via electrical resistivity tomography and mise-à-la-masse method. *Journal of Applied Geophysics*, 98, 1-10
- [6] Qarqori, K., Rouai, M., Moreau, F., Saracco, G., Dauteuil, O., Hermitte, D., Veslud, C. (2012). Geoelectrical Tomography Investigating and Modeling of Fractures Network around Bittit Spring (Middle Atlas, Morocco). *International Journal of Geophysics*, 2012, 1-13. doi: <https://doi.org/10.1155/2012/489634>
- [7] Ramazi, H., & Mostafaie, K. (2013). Application of integrated geoelectrical methods in Marand (Iran) manganese deposit exploration. *Arabian Journal of Geosciences*, 6, 2961-2970
- [8] Ferdows, S., & Ramazi, H. (2015). Application of the fractal method to determine the membership function parameter for geoelectrical data (case study: Hamy) copper deposit, Iran). *Journal of Geophysics and Engineering*, 12, 909-921
- [9] Mostafaie, K., & Ramazi, H. (2018). 3D model construction of induced polarization and resistivity data with quantifying uncertainties using geostatistical methods and drilling (Case study: Madan Bozorg, Iran). *Journal of Mining and Environment*, 9, 857-872. doi: <https://dx.doi.org/10.22044/jme.2018.6852.1516>
- [10] Yang, J., Liu, Z. H., & Wang, L. (2008). Effectiveness of Natural Field Induced Polarization for Detecting Polymetallic Deposits. *Earth Science Frontiers*, 15, 217-221
- [11] Flores, C., & Peralta-Ortega, S. (2009). Induced polarization with in-loop transient electromagnetic soundings: A case study of mineral discrimination at El Arco porphyry copper, Mexico. *Journal of Applied Geophysics*, 68, 423-436
- [12] Daneshvar Saein, L., Rasa, I., Rashidnejad Omran, N., Moarefvand, P., & Afzal, P. (2012). Application of concentration-volume fractal method in induced polarization and resistivity data interpretation for Cu-Mo porphyry deposits exploration, case study: Nowchun Cu-Mo deposit, SE Iran. *Nonlinear Processes in Geophysics*, 19, 431-438
- [13] Gurin, G., Tarasov, A., Ilyin, Y., & Titov, K. (2015). Application of the Debye decomposition approach to analysis of induced-polarization profiling data (Julietta gold-silver deposit, Magadan Region). *Russian Geology and Geophysics*, 56, 1757-1771.
- [14] Mashhadi, S., & Ramazi, H. (2018). The Application of Resistivity and Induced Polarization Methods in Identification of Skarn Alteration Haloes: a Case Study in the Qale-alimoradkhan Area. *Journal of Environmental and Engineering Geophysics*, 23(3), 363-368
- [15] Ögretmen, Z., & Şeren, A. (2014). Investigating fracture-cracked systems with geophysical methods in Bayburt Kırath travertine. *Journal of Geophysics and Engineering*, 11(6), 1-13. doi: <https://doi.org/10.1088/1742-2132/11/6/065009>
- [16] Grandjean, G., & Gourry, J. (1996). GPR data processing for 3D fracture mapping in a marble quarry (Thassos, Greece). *Journal of Applied Geophysics*, 36(1), 19-30. doi: [https://doi.org/10.1016/S0926-9851\(96\)00029-8](https://doi.org/10.1016/S0926-9851(96)00029-8)
- [17] Kadioğlu, S. (2008). Photographing layer thicknesses and discontinuities in a marble quarry with 3D GPR visualization. *J. Appl. Geophys.*, 64, 109-114. doi: <https://doi.org/10.1016/j.jappgeo.2008.01.001>
- [18] Porsani, L., Sauck, W., & Junior, A. (2006). GPR for Mapping fractures and as a guide for extraction of ornamental granite from a quarry: a case study from southern Brazil. *J. Appl. Geophys.*, 58, 177-187. doi: <https://doi.org/10.1016/j.jappgeo.2005.05.010>
- [19] Aydın, A., Yağız, S., Özpınar, Y., & Semiz, B. (2005, September 21-25). Investigation of travertine properties using geophysical methods. *Proceedings of 1st International Symposium on Travertine*.
- [20] Yalçınar, C. (2013). Investigation of subsurface geometry of fissure-ridge travertine with GPR, Pamukkale, western Turkey. *Journal of Geophysics and Engineering*, 10(3). doi: <https://doi.org/10.1088/1742-2132/10/3/035001>
- [21] Billi, A., Filippis, L., Poncia, P., Sella, P., & Faccenna, C. (2016). Hidden sinkholes and karst cavities in the travertine plateau of a highly-populated geothermal seismic territory (Tivoli, central Italy). *Geomorphology*, 255, 63-80. doi: <https://doi.org/10.1016/j.geomorph.2015.12.011>
- [22] Particle In Cell Consulting LLC (2015). *Finite Element Particle in Cell (FEM-PIC)*. Westlake village, CA. <https://www.particleincell.com/2015/fem-pic/>
- [23] Loke, M. H. (1996-2011). *Tutorial: 2-D and 3-D electrical imaging surveys*.
- [24] Chambers, J. E., Wilkinson, P. B., Wardrop, D., Hameed, A., Hill, I., Jeffrey, C., . . . Gunn, D. A. (2012). Bedrock detection beneath river terrace deposits using three-dimensional electrical resistivity tomography. *Geomorphology*, 17-25.
- [25] Doetsch, J., Linde, N., Vogt, T., Binley, A., & Green, A. G. (2012). Imaging and quantifying salt-tracer transport in a riparian groundwater system by means of 3D ERT monitoring. *GEOPHYSICS*, 207-218.
- [26] Uhlemann, S., Chambers, J., Wilkinson, P., Maurer, H., Merritt, A., Meldrum, P., Dijkstra, T. (2017). Four-dimensional imaging of moisture dynamics during landslide reactivation. *Journal of Geophysical Research: Earth Surface*, 398-418.
- [27] Blanchy, G., Saneiyani, S., Boyd, J., McLachlan, P., & Binley, A. (2020). ResIPy, an intuitive open-source software for complex geoelectrical inversion/modeling. *Computers & Geosciences*, 137. doi: <https://doi.org/10.1016/j.cageo.2020.104423>.

- [28] Binley, A. (2020). The Lancaster Environment Centre. Retrieved from <http://www.es.lancs.ac.uk/people/amb/Freeware/Freeware.htm>.
- [29] Geuzaine, C., & Remacle, J. F. (2009). Gmsh: A 3-D finite element mesh generator with built-in pre-and post-processing facilities. *International journal for numerical methods in engineering*, 1309-1331.
- [30] Abedi, M. (2020). A focused and constrained 2D inversion of potential field geophysical data through Delaunay triangulation, a case study for iron-bearing targeting at the Shavaz deposit in Iran. *Physics of the Earth and Planetary Interiors*, 309, 106604.
- [31] Abedi, M. (2022). Cooperative fuzzy-guided focused inversion for unstructured mesh modeling of potential field geophysics, a case study for imaging an oil-trapping structure. *Acta Geophysica*, DOI: 10.1007/s11600-022-00857-w.
- [32] Danaei, Kh., Moradzadeh, A., Norouzi, G.H., Smith, R.S., Abedi, M., & Jodeiri Akbari Fam, H. (2022). 3D inversion of gravity data with unstructured mesh and least-squares QR-factorization (LSQR). *Journal of Applied Geophysics*, DOI: 10.1016/j.jappgeo.2022.104781.
- [33] Talebi, M.A., Abedi, M., & Moradzadeh, A. (2022). Geoelectrical modeling of travertine rocks beneath a rough topographical relief using structured and unstructured meshes. *Acta Geodaetica et Geophysica*, 57, 351–372.
- [34] Telford, W. M., Geldart, L. P., & Sheriff, R. E. (1990). *Applied Geophysics*. Cambridge: Cambridge University Press. doi: <https://doi.org/10.1017/CBO9781139167932>.